Eur. Phys. J. B **46**, 309–314 (2005)
DOI: 10.1140/epjb/e2005-00263-7

THE EUROPEAN PHYSICAL JOURNAL B

Effects of the doping and the number of planes on the shadow bands of Bi-based cuprates

M. Izquierdo[1,2,a], L. Roca[1,3], J. Avila[1,3], G. Gu[4], Z.Z. Li[5], H. Raffy[5], and M.C. Asensio[2,3]

[1] LURE - Centre Universitaire Paris-Sud, Bât. 209D, 91898 Orsay Cedex, France
[2] Synchrotron SOLEIL- L'Orme des Merisiers, 91192 Gif-sur-Yvette Cedex, France
[3] Instituto de Ciencia de Materiales - CSIC, 28049 Madrid, Spain
[4] Brookhaven National Laboratory - Physics Department, Building 510B, Upton, New York 11975-5000, USA
[5] Laboratoire des Physiques des Solides - Centre Universitaire Paris-Sud, Bât. 510, 91405 Orsay Cedex, France

Received 20 January 2005 / Received in final form 29 April 2005
Published online 18 August 2005 –

Abstract. Angle resolved photoemission spectroscopy (ARPES) has been used to investigate the shadow bands present at the Fermi surface of bismuth based superconductors. $Bi_2Sr_2CaCu_2O_{8+\delta}$ (Bi2212) single crystals with different doping levels and $Bi_2Sr_2CuO_{6+\delta}$ (Bi2201) thin films have been studied by means of momentum distribution curves along the ΓY high symmetry direction in two different Brillouin zones and for an extensive photon energy range. The results show an enhancement of the shadow band intensity in the second Brillouin zone for photon energies around $h\nu = 30$ eV. Furthermore, the ratio *Shadow Bands/Main Band* is shown to be constant as a function of both the doping level and the number of CuO_2 planes. An interpretation of this observation on the basis of the current theoretical models will be provided.

PACS. 74.72.-h Cuprate superconductors (high-T_c and insulating parent compounds) – 71.18.+y Fermi surface: calculations and measurements; effective mass, g factor

1 Introduction

The study of the electronic properties of high T_c superconductors is one of the most active areas in material science research because it provides an essential test for the suitability of theoretical models developed to explain superconductivity. In particular, angle resolved photoemission spectroscopy (ARPES) and, more specifically, Fermi surface (FS) determination have proven to be a very powerful tool, which has contributed with a valuable wide-ranging experimental information to gain insight into the complex electronic properties of these compounds [1].

From the experimental point of view, although the electronic structure of most of the superconducting cuprate families have been studied by means of ARPES, a lot of research has been concentrated on the Bi compounds (and in particular the two plane compounds Bi2212) due to their laminar character which allows them to cleave very easily perpendicular to the c axis, thus providing clean and mirrorlike surfaces well suited for ARPES investigation. The Fermi surface of these compounds has shown to exhibit a large complexity with the presence of different sheets [1–3]. Besides the main bands (MB), we can also appreciate the existence of umklapp bands (UB) and Shadow bands (SB). The former are due to the $\mathbf{q} = \pm 0.21\mathbf{b}_0^*$ superstructure modulation present in these compounds while the origin of the SB still remains an open question, with two main different scenarios still under debate: antiferromagnetic correlations or structural distortions.

Evidences in favor of each scenario has been proposed both experimentally and theoretically. Theoretically, SB were predicted in two dimensional Hubbard model calculations performed in the weak coupling limit (on-site effective electron-electron Coulomb repulsion U smaller than the bandwidth W, U<W) [4], where they appear as a consequence of short-range antiferromagnetic correlations. Subsequent calculations within this framework have also supported the presence of SB [5,6] due to the antiferromagnetic fluctuations for correlation length as small as $x \sim 2a$ (a the lattice parameter) [5] and with a spectral weight that decreases as a function of doping [6]. However, other results have proposed that the correlation length should be comparable to the thermal wavelength of the electrons, a condition not fulfilled by these compounds [7]. On the other hand, SB have been also observed in two dimensional Hubbard models at half-filling as a consequence of spin singlet correlations [8,9]. Furthermore, *stripe* [10,11] and t-J model calculations have also obtained SB, although in some cases with a topology different from the experimentally observed one [11]. In the t-J calculations, they have been observed either as a

[a] e-mail: manuel.izquierdo@synchroton-soleil.fr

consequence of spin fluctuations in a large-degeneracy expansion [12] or analogous to the 1D holon band in exact diagonalization calculations [13], thus ruling out an antiferromagnetic origin. Finally, three dimensional Hubbard model calculations have shown that the SB at the Fermi surface, although always present, are boosted by antiferromagnetic correlations established between the two CuO_2 layers [14]. Considering the structural scenario, two different models have been proposed: on the one hand, the presence of a $c(2 \times 2)$ surface reconstruction was introduced by Chakravarty [15] on the basis that the short ranged antiferromagnetic correlations should give quasiparticles with a linewidth inversely proportional to the correlation length, while the observed SB are well defined. The other structural model is based on the slight orthorhombic distortion present in these materials [16], which upon breaking the tetragonal symmetry considers that the shadow bands are the main bands in a different orthorhombic Brillouin zone [17,18].

Regarding the experimental results, although a large amount of data exists in the literature and the SB are present in large portions of the Fermi surface, not many investigations have focused on them. Among the existing ones, we shall mention those supporting an antiferromagnetic scenario from Fermi surface measurements [3] or from the different behavior of the SB and main bands as a function of the binding energy [19] respectively. Regarding the orthorhombic distortion, the larger intensity of the SB detected in Pb-doped Bi2212 compared to non-doped ones [20] sustains this scenario [7] providing the orthorhombic distortion is larger in the former compounds [21,22]. Furthermore, studies as a function of doping have revealed a constant intensity ratio *shadow bands/main band* [23] which rules out the antiferromagnetic origin. This result has been recently questioned by measurements showing a direct relation between the SB and the superconductivity [24] due to the observed scaling between T_c and the shadow band intensity. The structural distortion scenario is also supported by the latest experiments showing the same behavior for the MB and SB with binding energy [25]. This observation does not agree with the results reported in reference [19] but it might be more reliable due to the fact that both the angular and energy resolution have been improved by a factor of 10. Finally, regarding the Bi2201 compounds, the SB have also been observed at the Fermi surface of these compounds [25,26]. Like the Bi2212 samples, they exhibit the same behavior with binding energy as the main bands, therefore supporting a structural origin [25]. In this context, recent VLEED results show the presence of a $c(2 \times 2)$ diffraction which indicates an important extrinsic contribution to the SB due to final state diffraction [27].

In this framework, we have to consider that most of the Fermi surface studies on cuprate superconductors have been restricted to the first Brillouin zone and to the borders of the second one close to it [1]. In this case, we have recently shown the SB to be more intense in the photon energy range (around $h\nu > 32$ eV) and for *odd* detection geometry [2,28]. From studies covering larger reciprocal

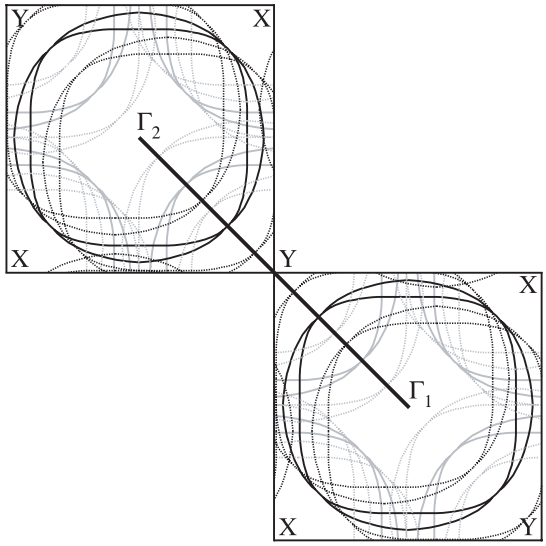

Fig. 1. Scheme of the first two tetragonal Brillouin zones for Bi cuprates together with a two hole-like FS adapted from measurements on an overderdoped Bi2212 single crystal [1]. Only those bands contributing to the $\Gamma_1 Y \Gamma_2$ have been included: main bands (gray lines), their umklapps (dashed gray lines), shadow bands (dark lines) and their umklapps (dashed dark lines).

space regions it has been observed that they exhibit very high intensity along the $Y\Gamma_2$ (see Fig. 1) of the second Brillouin zone [29,30]. Moreover, the SB intensity around this region seems to be maximal with respect to the other Brillouin zones, therefore becoming the best choice in order to investigate their properties. Furthermore, when one wants to compare the photointensity ratio with that of the Main Bands (MB) the $\Gamma_1 Y \Gamma_2$ is the only Brillouin zone direction along which there is no contribution of the umklapps bands, well separated in reciprocal space along this direction (see Fig. 1). On the other hand, it has the advantage that the two bands present in the Bi2212 compounds are degenerate. Therefore, $\Gamma_1 Y \Gamma_2$ is the only direction that allows a comparison between samples with different preparations, doping levels and number of CuO_2 planes. Measuring along others would imply the need to quantitatively evaluate the contribution of the umklapps, and to know precisely the nature of the two bands and their splitting in reciprocal space.

In this paper we present a systematic study of the shadow bands along the $\Gamma_1 Y \Gamma_2$ high symmetry direction by means of synchrotron radiation ARPES. In particular, the behavior of the SB intensity with photon energy has been extensively investigated thus allowing determination of the best experimental conditions for their study. Secondly, the behavior of the shadow bands with doping has been revisited in an attempt to clarify the controversy on the existing data. In this context, two Bi2212 single crystals at different doping level: optimal (OD) and underdoped 60 K (U60K) have been investigated. Finally, the dependence of the SB photointensity with the number of CuO_2 planes has also been elucidated by comparing

the results obtained in the above mentioned single crystals with those performed on a Bi2201 thin film grown on a $SrTiO_3$ single crystal.

2 Experimental details

The experiments were carried out at the Antares (SU8) Spanish-French beamline of Super-ACO storage ring at synchrotron LURE in Orsay, France. The beamline was equipped with a PGM monochromator made of six plane gratings, which covers an energy range from 16 eV to 960 eV with an average resolving power of 33×10^4 at a flux 10^{11} photons/s [2,31]. The end station is equipped with a high precision manipulator which allows a full 2π azimuthal angle (ϕ) rotation and a 90° polar angle (θ) variation relative to the surface normal, both with a precision higher than 0.5°. A VSW hemispherical analyzer mounted on a two-axis goniometer with an acceptance angle of 1° and an energy resolution of 50 meV is provided for the photoemission characterization [28,32]. A base pressure better than $P < 5 \times 10^{-11}$ mbar was kept during all the experiments. The samples were prepared by means of scotch cleavage, which has shown to provide the high quality mirror-like surfaces required for the experiment. An accurate in-situ sample alignment has been performed by photoelectron diffraction of the Bi $5d$ core level performed in the high kinetic energy regime, thus allowing to define the Γ point and the main high symmetry directions within our angular experimental resolution. Three different types of samples have been investigated: two single crystals of the Bi2212 family with different doping level and thin films of the Bi2201 one. The Bi2212 single crystals were grown by the travelling solvent floating zone method with an infrared mirror furnace. They exhibit a high crystalline quality as determined by X-ray diffraction and a sharp superconducting transition $\triangle T_c = 2$ K as determined from SQUIDS measurements [16]. They have different doping levels, one of them being optimally doped ($T_c = 91$ K) and the other underdoped with critical temperature $T_c = 60$ K. The Bi2201 thin film investigated belonged to the heavily overdoped regime ($T_c < 4.2$ K), it was epitaxially grown on $SrTiO_3$ by RF magnetron sputtering and its quality characterized by transport properties and X-Ray diffraction [33,34].

3 Results

We have performed a series of polar scans along the $\Gamma_1 Y \Gamma_2$ high symmetry direction. Since the analyzer is mounted on a two-axis goniometer, measurements can be performed in two different geometry detections, so-called *even* and *odd* [2,35]. In particular, the results presented here have been measured in the *even* detection geometry in which the surface normal, the direction of the outgoing electrons and the potential vector are coplanar. In this case and when measuring in a mirror plane of the crystal, as is the case for the $\Gamma_1 Y \Gamma_2$ direction, only those initial states having *even* symmetry will be detected.

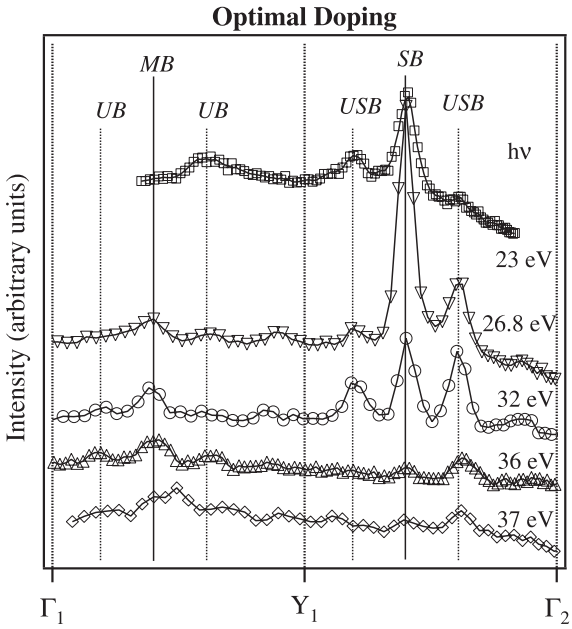

Fig. 2. Polar scans along the $\Gamma_1 Y \Gamma_2$ high symmetry direction for photon energies in the range from $h\nu = 23$ to $h\nu = 38$ eV for the Bi2212 optimally doped sample. Vertical lines correspond to the position of the main band (MB), umklapp bands (UB), shadow bands (SB) and their umklapps (USB) respectively.

In Figure 2 we present the polar scans measured along the $\Gamma_1 Y \Gamma_2$ high symmetry direction in the photon energy range between $h\nu = 23$ eV and $h\nu = 38$ eV for the Bi2212 at optimal doping. The results have been plotted together with lines indicating the Fermi level crossing of the different structures in the polar scans. These bands can be identified as follow: main band (MB), the umklapp bands corresponding to the $\mathbf{q} = \pm 0.21 \mathbf{b}_0^*$ superstructure modulation (UB), shadow bands (SB) and its corresponding $\mathbf{q} = \pm 0.21 \mathbf{b}_0^*$ umklapps (USB). At first glance, we can observe that the dominating photointensity arises from the SB and their umklapps in the second Brillouin zone ($Y\Gamma_2$ region), thus confirming to a large extent previous experimental results [29,30]. Moreover, we can establish a clear dependence of the intensity on the photon energy with three different energy ranges: for photon energies lower than $h\nu = 32$ eV, the photointensity in the second Brillouin zone is much larger than in the first one. Furthermore, concentrating on the second Brillouin zone only, we see that the dominant structure is that centered on the main shadow bands. Upon increasing the photon energy we can observe that the SB intensity on the second zone still dominates the spectrum, but the photointensity of their umklapps (USB) closer to Γ_2 starts becoming more important. Finally, for energies larger than $h\nu = 36$ eV the photointensity in the two Brillouin zones becomes similar. Regarding the second Brillouin zone, we see that the USB closer to Γ_2 is the dominating feature, which has also broadened with respect to lower photon energies.

We have further investigated this broadening by measuring a series of polar scans at the Fermi level (E_F), $E_F - 100$ meV and $E_F - 200$ meV for three different photon

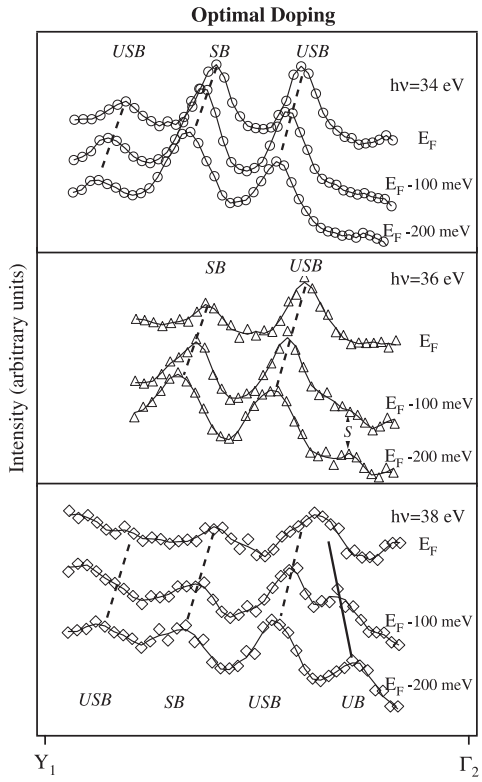

Fig. 3. Polar scans at the Fermi level, Fermi level-100 meV and Fermi level-200 meV along the YΓ_2 high symmetry direction for the Bi-2212 optimally doped sample. Three photon energies $h\nu$ = 34 (upper panel), 36 (intermediate panel) and 38 eV (lower panel) have been represented showing the increasing importance of the contribution arising from the main band umklapps (UB) as a function of the photon energy.

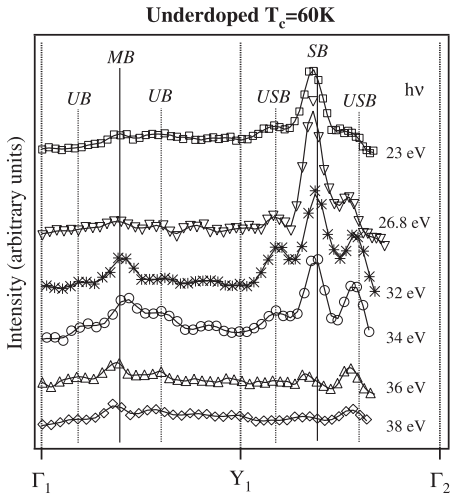

Fig. 4. Polar scans along the Γ_1 Y Γ_2 high symmetry direction for photon energies in the range from $h\nu$ = 23 to $h\nu$ = 38 eV for the underdoped T_c = 60 K Bi-2212 sample. Lines correspond to the position of the main band (MB), umklapp bands (UB), shadow bands (SB) and their umklapps (USB) have been also included.

energies $h\nu$ = 34 eV, $h\nu$ = 36 eV and $h\nu$ = 38 eV, which would allow us to discriminate the origin of the different structures by regarding their dispersion as a function of the momentum wavevector. Those structures dispersing towards the Γ_2 point can be ascribed to the SB and their umklapps as would correspond to holes centered at the Γ_2 points. On the contrary, the opposite dispersion is indicative of structures coming from the MB or their umklapps since in this case the holes are centered at the Y point. The results displayed in Figure 3 indicate a different behavior for the three photon energies measured. For the lowest photon energy $h\nu$ = 34 eV (upper panel) we only observe contributions coming from the shadow bands and their umklapps. Upon increasing the photon energy we observe that a shoulder is developing, denoted S in the intermediate panel. Finally, we see that the large broadening observed at $h\nu$ = 38 eV (lower panel) for the umklapp shadow band at the right side of the SB is due to the enhanced contribution of the structure "S" of panel b, which actually represents an umklapp of the main band (UB).

Figure 4 displays the polar scans measured for the other Bi2212 sample investigated, which belongs to the underdoped regime with a T_c = 60 K (U60K). We can observe that the polar scans resemble quite closely those obtained for the optimally doped sample(see Fig. 2). In particular, we can see that the intensity is dominating in the second Brillouin zone and also that the same three photon energy ranges are present at this doping level. The most striking difference is the fact that for this sample the umklapps bands are less intense than for the optimally doped sample, which could be ascribed to a weaker strength of the $\mathbf{q} = \pm 0.21\mathbf{b}_0^*$ incommensurate superstructure.

In order to investigate the behavior of the SB as a function of the number of CuO_2 planes we have performed measurements on a Bi2201 thin film grown on $SrTiO_3$. The use of these films has the advantage that the superstructure modulations are much weaker than on single crystals as observed by X-ray diffraction, thus reducing the complexity of the experimental Fermi surface. In Figure 5 the measured polar scans are displayed together with lines indicating the position of the expected structures in the two Brillouin zones, which have been labelled as in Figures 2 and 4. We observe that in this case the photointensity arising from the main band MB in the first Brillouin zone is always dominating over the rest of the structures, with an intensity that is lower for $h\nu$ = 23 eV and remains almost constant for the other energies. Furthermore, we can also see that for photon energies higher than 23 eV a broad shoulder in intensity develops between Γ_1 and the MB, which becomes more important as we increase the photon energy. On the contrary, and as expected, the umklapps bands are only weakly observed. Regarding the second Brillouin zone, we can distinguish three different situations: For $h\nu$ = 23 eV no evidence of the SB nor their umklapps is observed; for hν between 26.8 eV and 32 eV the SB are clearly seen and also their umklapps (USB), whose intensity is larger at 32 eV photon energy. Finally, for $h\nu$ = 38 eV the shadow band intensity washes out and only the USB closer to Γ_2 is left. Comparing these results

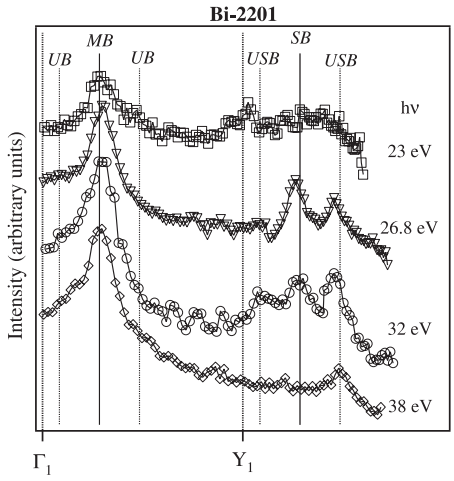

Fig. 5. Polar scans at the Fermi level for the Bi-2201 thin film. We observe that for very low photon energy no photointensity for the SB is present in the second Brillouin zone.

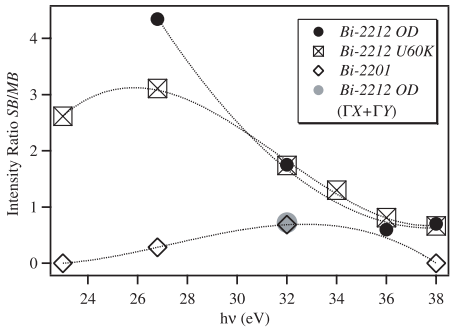

Fig. 6. Intensity ratio *SB/MB* as a function of the photon energy for the Bi-2212 and Bi-2201 samples.

with those obtained for the Bi2212 compounds we can infer that the behavior of the SB as a function of the photon energy in the second Brillouin zone is similar for high photon energies, while at low photon energies no photointensity was detected, which is opposite to the maximum observed for the Bi2212 compounds. The understanding of this experimental observation will be provided in the next section.

4 Discussion

Having presented all the experimental results, let us try to interpret them within the context of the existing scenarios. First of all, one can extract practical information regarding the optimal experimental conditions to study the SB for the different compounds. From the photon energy dependence we can infer that the energy range around $h\nu = 32$ eV will be optimal because the bands contributing to the photointensity are purely shadow bands and their umklapps. Furthermore, this photon energy range also allows comparison of the results for the two families investigated, which is not the case for the lowest photon energies for which the SB in the one plane compounds are not longer seen.

In order to obtain a physical understanding of the SB we have performed a quantitative estimation of the intensity ratio *SB/MB* as a function of the photon energy for the three different samples investigated (Fig. 6). We first notice that for a given sample there is an important variation of the intensity ratio with photon energy, as previously observed both theoretical and experimentally [2,35] and which might be ascribed to the angular dependence of the matrix elements since we observe that the photointensity dependence with photon energy for the SB is similar to that of the MB [36]. When comparing the results between Bi2212 samples with different doping levels we see that the ratio is constant for each photon energy, the only difference being the one obtained at $h\nu = 26.8$ eV. However, it is worth mentioning that this energy is a bit questionable in the sense that the Fermi level falls between a second order of Bi-5*d*, which could account for the observed differences. The constant ratio observed for the other photon energies indicates that the strength of the SB does not depend on the doping level. This result is in agreement with previous observations of Schwaller et al. [23] and does not agree with those of Kordyuk et al. [24] proposing a scaling of the SB intensity with the superconducting temperature T_c. A very intuitive interpretation of this observation would rule out an antiferromagnetic scenario, in which correlations should be enhanced upon reducing the doping level as theoretically observed [6].

Regarding the dependence with the number of CuO_2 planes, we can observe from Figure 6 that in principle the SB are much less intense compared to the Bi2212 single crystals. However, we have to keep in mind that for the Bi2201 samples the orthorhombic **a** and **b** axis are twinned, therefore we cannot perform a straightforward comparison of the obtained results. However, we can fairly compare the intensity ratio by considering the contributions coming from the ΓX and ΓY directions all together. As we can see from Figure 3 of reference [29], the photointensity along both high symmetry directions is quite different, mainly due to the presence of the umklapps along the ΓY direction. More concretely, the polar scans along the ΓX direction display a strong maximum in the first Brillouin zone while the intensity is very weak in the second one. Taking into account this effect we have estimated the intensity ratio of an artificial "ΓY+ΓX" polar scan at $h\nu = 32$ eV created by adding one ΓY to a ΓX polar scans. The result displayed in Figure 6 as a grey circle shows that the intensity ratio of this artificial polar matches precisely that measured for the Bi2201 sample. The consequence of this result is that the ratio *SB/MB* in the Bi samples can be considered as constant as a function of the number of CuO_2 planes. This observation contradicts the theoretical results obtained by Grabowski et al. [14]. These comes from a model supporting that, within an antiferromagnetic scenario, the coupling between layers plays a role in enhancing the SB intensity. Furthermore, this result is also against an orthorhombic distortion because we know that the distortion is much larger in the case

of the Bi2201 compounds, therefore a larger intensity ratio should be expected for this sample. In this context, our results are explicable by recalling the intense $c(2 \times 2)$ diffraction structure observed recently by VLEED [27], since we have observed a somewhat similar dependence with energy. However, they would support an origin for this $c(2 \times 2)$ diffraction structure based in a theoretically proposed surface reconstruction [15] rather than a consequence of the orthorhombic distortion. In any case, we believe that there is an important extrinsic contribution to the SB due to final-state diffraction.

5 Conclusions

In summary we have performed a systematic study of the shadow bands along the $\Gamma_1 Y \Gamma_2$ for both Bi2212 single crystals with different doping levels and Bi2201 thin films. The results have shown that the photon energy in the range from $h\nu = 26.8$ to 34 eV is best suited to investigate the shadow bands, since it allows a comparison not only within a family but among families with different numbers of copper-oxygen planes. Furthermore, we have obtained a constant behavior of the intensity ratio *shadow bands/main bands* as a function of both doping and the number of CuO_2 planes. The constancy as a function of doping rules out a link between the SB and the superconducting temperature and also questions the antiferromagnetic scenario. Finally, the constant behavior as a function of the number of copper oxygen planes has allowed us to discard a theoretical model sustaining a boosting of the shadow bands upon the interlayer coupling. This latter result also throws doubts on the orthorhombic explanation since the distortion appears to be more important for the one copper oxygen plane compounds and therefore a larger intensity ratio should be expected for the Bi2201 compounds. On the other hand, our results support an explanation based on the $c(2 \times 2)$ diffraction observed by VLEED and therefore related with final state diffraction effects.

Authors want to thank A. Bansil and M. Lindroos for the interesting discussions. This work has been financed by the Spanish MCYT project MAT2002-03431. Also, the Large-Scale Installation Program at LURE has partially supported this work under the grant number HPRI-CT-1999-00034. M.I. and L.R. thank Spanish MCYT for their fellowship.

References

1. A. Damascelli, Z-X Shen, Z Hussain, Rev. Mod. Phys. **75**, 473 (2003)
2. M.C. Asensio, J. Avila, L. Roca, A. Tejeda, G.D. Gu, M. Lindroos, R.S. Markiewicz, A. Bansil, Phys. Rev. B **67**, 014519 (2003)
3. P. Aebi, J. Osterwalder, P. Schwaller, L. Schlapbach, M. Shimoda, T. Mochiku, K. Kadowaki, Phys. Rev. Lett. **72**, 2757 (1994)
4. A. Kampf, J.R. Schrieffer, Phys. Rev. B **41**, 6399 (1990); A. Kampf, J.R. Schrieffer, Phys. Rev. B **42**, 7967 (1990)
5. A.V. Chubukov, Phys. Rev. B **52**, R3840 (1995)
6. S. Haas, A. Moreo, E. Dagotto, Phys. Rev. Lett. **74**, 4281 (1995)
7. Y.M. Vilk, Phys. Rev. B **55**, 3870 (1997)
8. S. Onoda, M. Imada, Phys. Rev. B **67**, 161102 (2003)
9. F.F. Assaad, M. Imada, Eur. Phys. J. B **10**, 595 (1999)
10. M. Moraghebi, C. Buhler, S. Yunoki, A. Moreo, Phys. Rev. B **63**, 241513 (2001)
11. M.I. Salkola, V.J. Emery, S.A. Kivelson, Phys. Rev. Lett. **77**, 155 (1996)
12. M.F. Bishop, Z.P. Gibbs, T. McMullen, Phys. Rev. B **59**, 14937 (1999)
13. R. Eder, Y. Ohta, Phys. Rev. B **56**, 2452 (1997)
14. S. Grabowski, J. Schmalian, K.H. Bennermann, Solid Stat. Comm. **102**, 493 (1997)
15. S. Chakravarty, Phys. Rev. Lett. **74**, 1885 (1995)
16. G. Gu, K. Takamuku, N. Koshizuka, S. Tanaka, J. Crystal Growth **130**, 325 (1993)
17. D.J. Singh, W.E. Pickett, J. Superconductivity **8**, 583 (1995); Phys. Rev. B **51**, 3128 (1995)
18. W.E Pickett, Rev. Mod. Phys. **61**, 433 (1989)
19. S. LaRosa, R.J. Kelley, C. Kendziora, G. Margaritondo, M. Onellion, A. Chubukov, Solid State Comm. **104**, 459 (1997)
20. H.M. Fretwell, A. Kaminski, J. Mesot, J.C. Campuzano, M.R. Norman, M. Randeria, T. Sato, R. Gatt, T. Takahashi, K. Kadowaki, Phys. Rev. Lett. **84**, 4449 (2000)
21. P. Aebi, J. Osterwalder, P. Schwaller, H. Berger, C. Beeli, L. Schlapbach, J. Phys. Chem. Solids **56**, 1845 (1995)
22. P. Schwaller, P. Aebi, H. Berger, C. Beeli, J. Osterwalder, L. Schlapbach, J. Elec. Spec. Rel. Phen. **76**, 127 (1995)
23. P. Schwaller, T. Greber, P. Aebi, J.M. Singer, H. Berger, L. Forró, J. Osterwalder, Eur. Phys. J. B **18**, 215 (2000)
24. A.A. Kordyuk, S.V. Borisenko, M.S. Golden, S. Legner, K. A. Nenkov, M. Knupfer, J. Fink, H. Berger, L. Forró, R. Follath, Phys. Rev. B **66**, 014502 (2002)
25. A. Koitzsch, S. V. Borisenko, A. A. Kordyuk, T. K. Kim, M. Knupfer, J. Fink, M. S. Golden, W. Koops, H. Berger, B. Keimer, C. T. Lin, S. Ono, Y. Ando, R. Follath, Phys. Rev. B **69**, R220505 (2004)
26. R. Müller, C. Janowitz, M. Schneider, A. Krapf, H. Dwelk, R. Manzke, Physi. C **341-348**, 2109 (2000)
27. V.N. Strocov, R. Claessen, P. Blaha, Phys. Rev. B **68**, 144509 (2003)
28. M. Izquierdo L. Roca, D.G. Gu, J. Avila, M.C. Asensio, Appl. Surface Sci. **212-213**, 67 (2003)
29. N.L. Saini, J. Avila, A. Bianconi, A. Lanzara, M.C. Asensio, S. Tajima, G.D. Gu, N. Koshizuka, Phys. Rev. Lett. **79**, 3467 (1997)
30. A. Bianconi, N.L. Saini, A. Valletta, A. Lanzara, J. Avila, M.C. Asensio, S. Tajima, G.D. Gu, N. Koshizuka, J. Phys. Chem. Solids **59**, 1884 (1998)
31. M.E. Dávila, S.L. Molodtsov, M.C. Asensio, C. Laubschat, Phys. Rev. B **62**, 1635 (2000)
32. L. Roca, M. Izquierdo, A. Tejeda, D.G. Gu, J. Avila, M.C. Asensio, Appl. Surface Sci. **212-213**, 62 (2003)
33. Z.Z. Li, H. Rifi, A. Vaures, S. Megtert, H. Raffy , Phys. C **206**, 367 (1993)
34. Z. Konstantinovic, Z.Z. Li, H. Raffy, Phys. C **351**, 163 (2001)
35. A. Bansil, M. Lindroos, S. Sahrakorpi, R.S. Markiewicz, G.D. Gu, J. Avila, L. Roca, A. Tejeda, M.C. Asensio, J. Phys. Chem. Solids **63**, (2002) 2175.
36. S. Sahrakorpi, M. Lindroos, A. Bansil Phys. Rev. B **68**, 054522 (2003)